Journal of Materials Chemistry A

How does a Small Structural Change of Anode Ionomer Make a Big Difference in Alkaline Membrane Fuel Cell Performance?

Journal:	*Journal of Materials Chemistry A*
Manuscript ID	TA-ART-09-2019-010157.R1
Article Type:	Paper
Date Submitted by the Author:	30-Sep-2019
Complete List of Authors:	Park, Eun Joo; Los Alamos National Laboratory, Maurya, Sandip; Los Alamos National Laboratory, MPA-11: Materials Synthesis and Integrated Devices Lee, Albert; Los Alamos National Laboratory, MPA-11: Materials Synthesis and Integrated Devices Leonardo, Daniel; Los Alamos National Laboratory, MPA-11: Materials Synthesis and Integrated Devices Li, Dongguo; Los Alamos National Laboratory, MPA-11: Materials Synthesis and Integrated Devices Jeon, Jong Yeob; Rensselaer Polytechnic Institute, Department of Chemistry and Chemical Biology Bae, Chulsung; Rensselaer Polytechnic Institute, Department of Chemistry and Chemical Biology Kim, Yu Seung; Los Alamos National Laboratory, MPA-11: Materials Synthesis and Integrated Devices

ARTICLE

Received 00th January 20xx,
Accepted 00th January 20xx
DOI: 10.1039/x0xx00000x

How does a Small Structural Change of Anode Ionomer Make a Big Difference in Alkaline Membrane Fuel Cell Performance?

Eun Joo Park,‡[a] Sandip Maurya,‡[a] Albert S. Lee,[a] Daniel P. Leonard,[a] Dongguo Li,[a] Jong Yeob Jeon,[b] Chulsung Bae[b] and Yu Seung Kim*[a]

Anode ionomers of alkaline membrane fuel cells (AMFCs) play a critical role in hydrogen and water transport thus affecting cell performance and durability. Here, we modified a quaternized poly(biphenyl alkylene) ionomer with two chemical structural variations to increase hydrogen access to the AMFC anode: first, we introduced the symmetric dimethyl groups in the polymer backbone to increase polymer fractional free volume. Second, we replaced hydroxide-conducting alkyl trimethylammonium with alkyl triethylammonium to reduce cation-hydroxide-water co-adsorption on the hydrogen oxidation catalyst to increase hydrogen access to the co-adsorbed layer. We compared the performance benefits of the two structural variations through operating AMFCs under H_2/O_2 conditions. The membrane electrode assembly employing the modified poly(biphenyl alkylene) ionomer at the anode exhibited > 1,500 mW cm^{-2} peak power density at 80 °C with stable short-term durability (> 100 h) under a constant current density of 0.6 A cm^{-2}. This study provides an essential insight into designing anode ionomer of high-performance AMFCs.

Introduction

Alkaline-stable and high performing polymer electrolyte is a crucial requirement for advanced alkaline membrane fuel cells (AMFCs).[1] Although many efforts have been devoted to the development of anion exchange membrane (AEM) separators over the past decade,[2-15] the polymer electrolytes for catalyst layers (ionomers) have received less attention,[16-18] and the role of ionomers on the AMFC performance and durability has been underestimated.

In general, alkaline ionomers require high hydroxide conductivity, high reactant gas permeability, and excellent alkaline stability. In addition to these, recent research from our group has indicated that dissimilar ionomer structures at the anode and the cathode may be required for the best-performing AMFCs.[19-22] Since the oxygen reduction reaction (ORR) consumes water at the AMFC cathode, electrode flooding is less significant compared to that of proton-exchange membrane fuel cells. Instead, acidic phenol formation from the oxidation of the ionomer is the most detrimental factor affecting AMFC performance and durability[19, 22] The acidic phenol from phenyl oxidation lowers the local pH at the ORR catalyst/ionomer interface.[19-22] At the AMFC anode, on the other hand, one of the most significant issues may be phenyl group adsorption on the surface of hydrogen oxidation reaction (HOR) electrocatalysts.[20, 21] Strong adsorption of the phenyl group parallel to the metal surface due to the favourable interaction of aromatic π-electrons of the phenyl group blocks the catalyst active sites of HOR. Fortunately, follow-up research has shown that the adverse impact of the phenyl group adsorption could be mitigated by using less-phenyl group adsorbing ionomers.[23] Furthermore, Pt-Ru bimetallic catalysts can efficiently reduce the phenyl group adsorption through the electronic structure change of Pt atoms.[20] Several papers have shown excellent performance of Pt-Ru anode catalyzed AMFCs.[24, 25] When the effect of phenyl adsorption is minimal, the next significant issue of the AMFC anode would be low hydrogen accessibility to the HOR catalyst. The hydrogen transport issue at the AMFC anode is not only due to the low hydrogen permeation rate of excess generation of water,[26] but also due to the local hydrogen transport resistance at the catalyst/ionomer interface through the cumulative cation-hydroxide-water co-adsorption on HOR catalysts.[27] Some research efforts have been made to improve hydrogen transport by polyolefinic ionomers with partially fluorinated hydrophobic polymer backbone, *i.e.,* poly(ethylene-*co*-tetrafluoroethylene), and increased porosity by the powder form ionomeric binders.[16, 28] However, there is limited study into polyaromatic ionomers to improve hydrogen gas transport. Furthermore, there is no attempt to reduce cation-hydroxide-water co-adsorption by altering the chemical structure of ionomeric binders so far.

[a] *MPA-11: Materials Synthesis & Integrated Devices, Los Alamos National Laboratory, Los Alamos, New Mexico 87545, USA. E-mail: yskim@lanl.gov*
[b] *Department of Chemistry and Chemical Biology, Rensselaer Polytechnic Institute, Troy, New York 12180, USA*
† Electronic supplementary information (ESI) available: Fig. S1-S5. See DOI: 10.1039/x0xx00000x
‡ These authors contributed equally to this work.

Here, we demonstrate an anode ionomer design strategy to improve AMFC performance, focusing on enhancing hydrogen transport. We implemented two design strategies for quaternized polyaromatic ionomers: the first approach is to substitute phenyl hydrogen in the ionomer backbone with symmetric methyl groups. This idea came from the classic theory of gas separation membranes that symmetric methyl substitution can restrict the internal rotation around the bonds between the phenyl rings to increase the fractional free volume (FFV), thus efficiently increasing hydrogen permeability.[29, 30] The second approach is to replace trimethylammonium (TMA) functional group to the bulkier cationic groups such as triethylammonium (TEA). This idea came from the rotating disk electrode (RDE) experiments and density functional theory calculations that showed that the adsorption energy of TEA

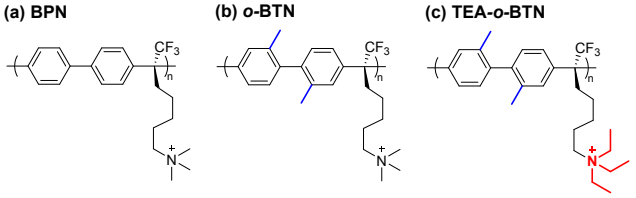

Fig. 1 The chemical structure of quaternized poly(biphenyl alkylene)s.

on catalysts is much smaller due to the steric hindrance of the bulkier alkyl groups, which do not allow for favourable positioning of the bulky cation on the surface of electrocatalysts as TMA does.[31, 32] Finally, we show how the structural change of anode ionomers impacts the AMFC performance and short-term durability.

Results and Discussion

Molecular design of quaternized poly(biphenyl alkylene)s

We have chosen poly(biphenyl alkylene) (BPN) ionomers as a base material (Fig. 1a).[33] These aryl ether-free quaternized polyaromatics are known for their excellent alkaline stability and good solubility among quaternized polyaromatics, which make them desirable for the ionomeric materials in the catalyst layer.[34] The first structural variation was achieved by symmetric dimethyl substitution of the biphenyl group in the polymer backbone, *i.e.,* poly(*o,o'*-bitolyl alkylene) (*o*-BTN) (Fig. 1b). Based on the modified free volume-based group contribution method,[35] FFV of the bromoalkyl-tethered poly(*o,o'*-bitolyl alkylene) (*o*-BTBr) was calculated to be 20.2%, which is higher than that of the bromoalkyl-tethered poly(biphenyl alkylene), BPBr (16.7%). The hydrogen permeability coefficient, P_{H2} is estimated from the following empirical equation:

$$P_{H2}\,(Barrer) = A\exp\left(-\frac{B}{FFV}\right),$$

$$A = 1{,}070 \; and \; B = 0.643 \; at \; 35\,^{\circ}\mathrm{C}, 2 \; atm$$

The estimated P_{H2} of *o*-BTBr and BPBr is 44.6 and 22.9 Barrer, respectively.

The second structural variation was achieved by replacing the TMA group in *o*-BTN with the TEA group (TEA-*o*-BTN) (Fig. 1c). Neutron reflectometry experiments[36] showed that the cation-hydroxide-water co-adsorbed layer thickness of TEA hydroxide

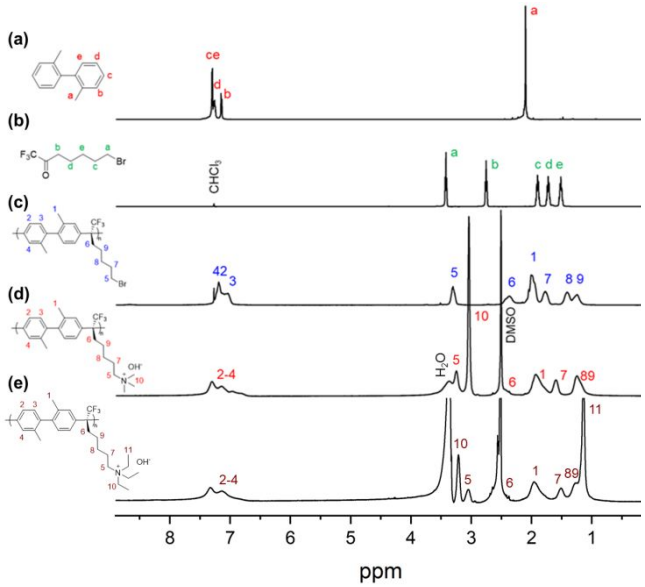

Fig. 2 ^{1}H NMR spectra of (a) *o,o'*-bitolyl, (b) ketone monomer, (c) *o*-BTBr in $CDCl_3$, (d) *o*-BTN and (e) TEA-*o*-BTN in DMSO-d_6.

(TEAOH) on polycrystalline Pt is 5 Å, which is significantly thinner than that of TMA hydroxide (TMAOH) (16 Å) after 4.5 h exposure at 0.1 V *vs.* Reverse Hydrogen Electrode (RHE). After 12-hour exposure at 0.1 V *vs.* RHE, the co-adsorbed layer thickness of TEAOH increases to 7 Å, which is only ~40% of the TMAOH thickness. As the cation composition in the co-adsorbed layer is similar, *ca*. ammonium hydroxide to water ratio is approximately 5 to 1, the hydrogen permeation of the TEAOH co-adsorbed layer is 2.5–3.2 fold higher than that of the TMAOH co-adsorbed layer.

The *o*-BTN and TEA-*o*-BTN ionomers were synthesized *via* the polycondensation reaction of bromopentyl trifluoromethyl ketone and *o,o'*-bitolyl followed by Menshutkin reaction to substitute terminal bromo groups into ammonium functional groups. The bromoalkyl-tethered precursor copolymer (*o*-BTBr) was prepared by acid-catalyzed Friedel-Crafts polycondensation using the prepared monomers.[33, 37] The *o*-BTBr precursor showed good solubility in most organic solvents including chlorinated solvents and tetrahydrofuran while remaining insoluble in dimethylsulfoxide (DMSO), low molecular weight alcohols and water. The chemical structure of monomers and *o*-BTBr was characterized by ^{1}H NMR spectroscopy (Fig. 2a-c). The ionic *o*-BTN and TEA-*o*-BTN was formed *via* S_N2 reaction of TMA and TEA to convert the bromopentyl group of *o*-BTBr into ammonium bromide, respectively. Comparison of the relative area of the proton of TMA at 3.04 ppm (TEA at 3.20 ppm) and the -CH_3 proton peaks of the backbone at 1.93 ppm in the ^{1}H NMR spectra indicated that the quaternization reaction gave quantitative conversion (Fig. 2de). The ion exchange capacity (IEC) of *o*-BTN, TEA-*o*-BTN and BPN determined by ^{1}H NMR spectroscopy was 2.5, 2.2 and 2.6 meq. g^{-1}, respectively (Table 1).

The ionomers were characterized in terms of their solubility, water uptake, conductivity, and alkaline stability (Table 1). The solubility of hydroxide form ionomer is crucial to process impurity-free electrode fabrication. The hydroxide form of BPN, *o*-BTN and TEA-*o*-BTN showed good solubility in a wide range of polar solvents

Table 1 Water uptake, ion conductivity and IECs[a]

Ionomer	Water uptake (%)[b]	Conductivity (mS cm^{-1})[c]	Initial IEC (meq. g^{-1})	IEC after 114 h (meq. g^{-1})[d]	IEC after 500 h (meq. g^{-1})[d]
BPN	130[e]	0.83	2.6[e]	--	2.6[ef]
o-BTN	119	0.89	2.5	--	2.5[g]
TEA-*o*-BTN	94	1.05	2.2	2.1 (3.5% decrease)	2.0 (11% decrease)

[a] Measured by ^{1}H NMR calculation. [b] Measured in OH^- form at room temperature. [c] Solution conductivity was measured at $[QA^+]$ = 0.16 M in anhydrous DMSO. [d] after the alkaline stability test (1 M NaOH, 80 °C). [e] Taken from Ref. 31. [f] IEC after 720 h. [g] No change detected in the ^{1}H NMR spectrum.

including methanol, ethanol, ethylene glycol and polar aprotic solvents, while remaining insoluble in water and less polar organic solvents. The water uptake of ionomers in OH^- form was measured at room temperature, and the ionomer with the higher concentration of the ionic groups showed the higher water uptake. The ion conductivity is typically measured in OH^- ion exchanged-membrane form. However, as high performance ionomeric binders used in fuel cells do not form freestanding films, we measured solution conductivity of ionomers in anhydrous DMSO at the same molar concentration at 80 °C for comparison.[38] As a baseline, the ionic conductivity of 0.16 M BPN was measured to be 0.83 mS cm^{-1} in DMSO, which corresponds to the value of 127 mS cm^{-1} of a membrane form of the ionomer in water according to our previous study.[33] *o*-BTN and TEA-*o*-BTN showed slightly higher conductivity: 0.89 mS cm^{-1} for *o*-BTN and 1.05 mS cm^{-1} for TEA-*o*-BTN. The slightly higher ion conductivity may be related to the dispersion morphology of the ionomer in DMSO. This result suggests that the *o*-BTN and TEA-*o*-BTN ionomers in the electrode may have comparable hydroxide conductivity with BPN. The chemical stability of the ionomers was evaluated by measuring the IEC change after immersing the ionomers in 1 M NaOH at 80 °C using ^{1}H NMR spectroscopy (Fig. 3). While we could not detect any changes in the spectra of BPN and *o*-BTN, the IEC of TEA-*o*-BTN decreased from 2.2 to 2.0 meq. g^{-1} after 500 h of the stability test. The decrease of the relative area of the peak at 3.20 ppm (Fig. S1, 5.3H, originally 6H) indicates the degradation of the ethyl group caused by the E2 elimination mechanism,[39, 40] which agrees with the cation stability reported in the literature.[41]

Impact of dimethyl substitution on H_2 diffusion and AMFC performance

To investigate the effect of dimethyl substitution on hydrogen permeability of the ionomer, we measured the H_2 diffusion coefficient of ionomers in H_2 gas saturated DMSO dispersions by the pulsed-field-gradient ^{1}H NMR technique. In this measurement, we saturated a 2 wt% ionomer dispersion in dry DMSO-d_6 with ultra-high purity H_2, of which we could observe a distinctive singlet peak at ~4.5 ppm for H_2 (Fig. S2).[42, 43] Using a well-known self-diffusion coefficient measurement explained by Krishnan[44] and others,[45-47] the H_2 diffusion coefficients of BPN and *o*-BTN dispersions were calculated through fits of the diffusion-dependent H_2 signal attenuation (example shown in Fig. S3) as a function of diffusion delay. A summary of the H_2 diffusion coefficients for BPN and *o*-BTN as a function of temperature is depicted in Table 2. While the H_2 concentration dissolved in the ionomer dispersions were very similar, the difference in the H_2 diffusion coefficient between quaternized BPN and *o*-BTN was about 4 folds at 40 °C. Considering that the estimated H_2 permeability of non-quaternized *o*-BTN based on FFV theory is about 2 times greater than that of non-quaternized BTN at 35 °C, the result suggests that there were additional effects derived from the quaternization and dispersion morphology. The difference in H_2 diffusion coefficient further increases with temperature: about five fold difference at 80 °C. The significantly increased H_2 diffusion coefficient with symmetric dimethyl substitution supports our rationale in designing the ionomer backbone structure to enhance H_2 permeation.

Table 2 Self-diffusion coefficients of H_2 in BPN and *o*-BTN dispersions

Temperature (°C)	Self-diffusion coefficient (D) of H_2 (10^{-9} m^2 s^{-1})		
	BPN	*o*-BTN	TEA-*o*-BTN
25	2.7	8.0	9.4
40	3.2	12.5	14.4
65	3.8	17.6	19.9
80	4.5	22.3	24.2

We compared the AMFC performance of MEAs employing the BPN and *o*-BTN polymer electrolytes at the anode. For this comparison, we have used the same MEA components except for the anode ionomeric binder. We used the same quaternized poly(*m*-terphenylene) (*m*-TPN) AEM[48] with the thickness of 35 μm (Figure S4). Similar cell high-frequency resistance (HFR) for all MEAs suggests that ohmic resistance of the AEM and humidification for all MEAs have negligible difference. For Pt/C anode catalyzed MEAs (Fig. 3a), the peak power density of the *o*-BTN-based MEA was 450 mW cm^{-2}, ~25% higher than that of the BPN-based MEA. Note that the performance difference started at the current density of 0.4 A cm^{-2}, suggesting that the kinetic performance of the MEAs was similar, yet the H_2 transport made the difference in performance. For the Pt-Ru/C anode catalyzed MEAs (Fig. 3b), the fuel cell performance of both MEAs significantly improved confirming that phenyl group adsorption is still one the most significant performance limiting factors for the polyaromatic-based MEAs.[20] With Pt-Ru/C anode, the peak power density of the *o*-BTN-based MEA was 780 mW cm^{-2}, ~25% higher than that of the BPN. The same degree of improvement with the *o*-BTN-based MEA suggests that the AMFC performance improvement may be originated from the high H_2 permeability of the *o*-BTN ionomer. Relatively small performance improvement with the *o*-BTN ionomer in spite of the ~5 times higher hydrogen diffusion coefficient suggests that the hydrogen transport through the thin film electrode has a partial contribution to the overall AMFC

performance. Nonetheless, the result indicated that the notable AMFC performance improvement can be made by increasing the hydrogen diffusion rate of anode polymer electrolytes.

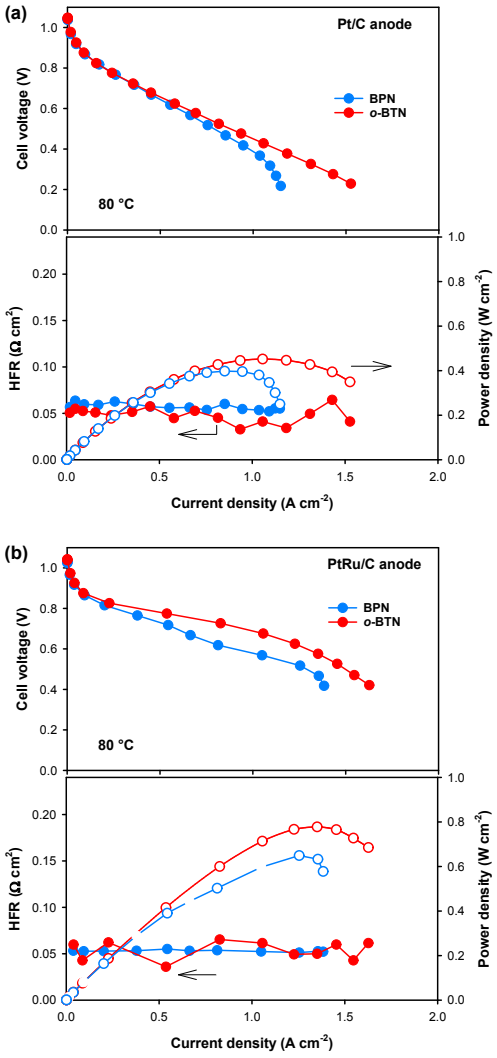

Fig. 3 Impact of *o*-BTN anode ionomer on AMFC performance of (a) Pt anode catalysed and (b) Pt-Ru/C anode catalysed MEAs. Measured the performance at 80 °C under fully humidified H_2/O_2 (500/300 sccm) at 285 kPa backpressure. AEM: *m*-TPN (35 µm, IEC = 2.1 meq. g^{-1}); anode: Pt/C (0.6 mg_{Pt} cm^{-2}) or Pt-Ru/C (0.5 mg_{Pt} cm^{-2}); cathode: Pt/C (0.6 mg_{Pt} cm^{-2}) with BPN ionomer.

Impact of triethylammonium functionalization on H_2 permeability and AMFC performance

Since cation-hydroxide-water co-adsorption is cumulative and occurs at the interface between the ionomer and HOR catalyst, H_2 permeability through the co-adsorbed layer would not be measured by H_2 permeability of bulk membranes. Therefore, we investigated the H_2 transport of the co-adsorbed layer using RDE and ionomer-coated microelectrode half-cell, of which methods are well documented in our previous publications.[27, 31, 49]

Fig. 4a shows the HOR voltammograms acquired for Pt/C in 0.1 M TMAOH and TEAOH. After the preconditioning at 1.4 V vs. RHE, the HOR currents in the organic electrolytes at low cell voltage were similar, ca. 43 mA cm^{-2} at 0.01 V, suggesting little, if any, difference in the interaction between the different cations and the Pt surface.

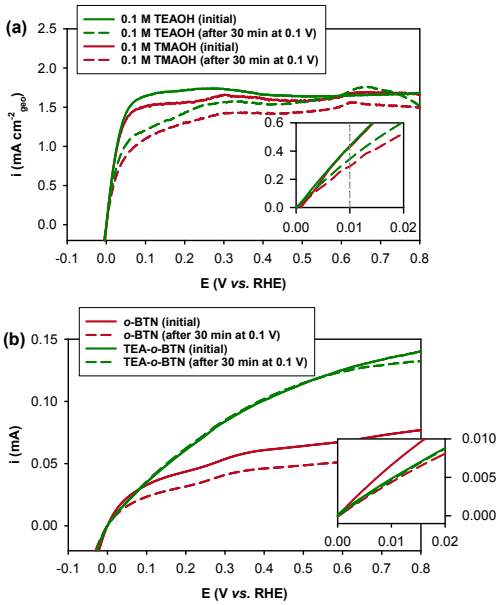

Fig. 4 (a) HOR voltammograms of Pt/C RDE in 0.1 M TMAOH and 0.1 M TEAOH; HOR voltammogrrams were recorded at 25 °C, rotating speed: 900 rpm, scan rate: 5 mVs^{-1} pre-conditioning at 1.4 V *vs.* RHE for 30 s (initial) and after chronoamperometry at 0.1 V *vs.* RHE for 30 min. (b) HOR voltammograms of *o*-BTN- and TEA-*o*-BTN-coated Pt microelectrode. The voltammograms were recorded after pre-conditioning at 1.4 V *vs.* RHE for 20 s (initial) and after chronoamperometry at 0.1 V *vs.* RHE for 30 min.

However, notably higher current density for Pt/C in 0.1 M TEAOH was observed as the cell voltage increased until the current density became similar at ~0.6 V. For example, the current density of Pt/C in 0.1 M TEAOH was 1.63 mA cm^{-2} at 0.1 V while the current density of Pt/C in 0.1 M TMAOH was 1.52 mA cm^{-2}. After exposing the electrode at 0.1 V *vs.* RHE for 30 min, Pt/C RDE both in the TMAOH and TEAOH solutions exhibited decreased HOR activity due to the cumulative adsorption of cation-hydroxide-water. This result indicates that the adsorption of the TEA cations on Pt/C is less and the hydrogen transport through the TEA co-adsorbed layer is faster.

Next, we investigated the hydrogen transport through the *o*-BTN and TEA-*o*-BTN ionomers. Fig. 4b shows the HOR voltammograms of Pt/C in contact with *o*-BTN and TEA-*o*-BTN thin film (approx. 0.5 µm thick) from 0.0 to 0.8 V vs. RHE after pre-treatment of the microelectrode at 1.0 V vs. RHE for 20 s and exposure of the microelectrode at 0.1 V vs. RHE for 30 min (Fig. 4a). The intrinsic HOR activity of the Pt/C microelectrode in contact with *o*-BTN and TEA-*o*-BTN was determined by the slope between 0 and 0.01 mA. It was found that the intrinsic activity of the Pt/C microelectrode in contact with *o*-BTN and TEA-*o*-BTN were similar regardless of the pre-treatment conditions. After pre-conditioning at 1.4 V vs. RHE for 30 s., the current density of TEA-*o*-BTN coated Pt/C microelectrode is significantly higher at > 0.05 V, suggesting that TEA co-adsorption on

the Pt/C microelectrode is much less than TMA co-adsorption. As a result, the limiting current density of TEA-*o*-BTN-coated Pt/C microelectrode determined at 0.8 V *vs.* RHE for *o*-BTN is 1.8-times higher than that of *o*-BTN. After exposing the microelectrode at 0.1 V *vs.* RHE, the limiting current of the ionomer-coated microelectrodes decreased due to the cumulative cation-hydroxide-water co-adsorption. The hydrogen diffusion rate of the *o*-BTN thin film after the exposure at 0.1 V for 30 min is ~ 2.2 times smaller than that of TEA-*o*-BTN. One should note that the H_2 permeability of the co-adsorbed layer with tens of angstrom thickness is a few orders of magnitude lower than the H_2 permeability in pure water due to substantially high ammonium concentration.[50]

The AMFC performance of MEAs using BPN, *o*-BTN and TEA-*o*-BTN anode ionomers was compared under H_2/O_2 conditions (Fig. 5a). The improved peak power density of the *o*-BTN-based MEA (780 mW cm^{-2}) from the BPN-based MEA further increased with the TEA-*o*-BTN-based MEA (1,278 mW cm^{-2}, ~60% higher than the MEA employing *o*-BTN). The similar cell HFR values between the cells suggested that the initial performance difference came from the anode rather than the AEM humidification. Like the case observed with the performance of MEA using the BPN and *o*-BTN ionomers, the improved performance was achieved at higher cell current density, confirming that the reason for the performance improvement is related to the H_2 reactant transport rather than the catalyst kinetic activity change. This is consistent with the RDE and microelectrode results in which the notable HOR performance differences were observed at a higher anode potential, ca. > 0.01 V *vs.* RHE. Additional increase in the H_2 flow rate further improved the AMFC performance. With 2,000 sccm of H_2 gas flowing, the peak power density of the AMFC reached > 1,500 mW cm^{-2}, comparable to the best-performing polyaromatic-based AMFC performance reported in the literature.[14, 15, 23] Comparing the AMFC performance of an MEA employing fluorene-based ionomer (FLN, Figure S4)[23], the MEA using the TEA-*o*-BTN ionomer showed inferior performance at high cell voltage (Fig. S5); for example, the current density at 0.8 V of the FLN-based MEA was 0.623 A cm^{-2}, 47% higher than that of the TEA-*o*-BTN (0.423 A cm^{-2}). However, the AMFC performance of the TEA-*o*-BTN-based MEA at low cell voltage is superior to that of the FLN-based MEA; for example, the current density at 0.5 V of the TEA-*o*-BTN-based MEA was 3.06 A cm^{-2}, 8% higher than that of the FLN-based MEA (2.84 A cm^{-2}). This result suggests that the performance improvement using the FLN ionomer was achieved by minimizing the adverse phenyl adsorption on HOR catalyst, which impacts the kinetic performance of AMFC while the performance improvement using the TEA-*o*-BTN ionomer was accomplished by higher hydrogen transport.

The impact of anode ionomer on the short-term durability of AMFC was investigated. For the short-term durability evaluation, we have run the three MEAs employing BPN, *o*-BTN and TEA-*o*-BTN anode ionomers for 120 h at 80 °C and a constant current density of 0.6 A cm^{-2}. During the short-term test, we did not alternate cell voltage or replenish the cell with alkali metal solutions which typically makes the cell performance recover by the desorption of cation-hydroxide-water from the surface of HOR catalysts.[19] Fig. 5b shows the cell

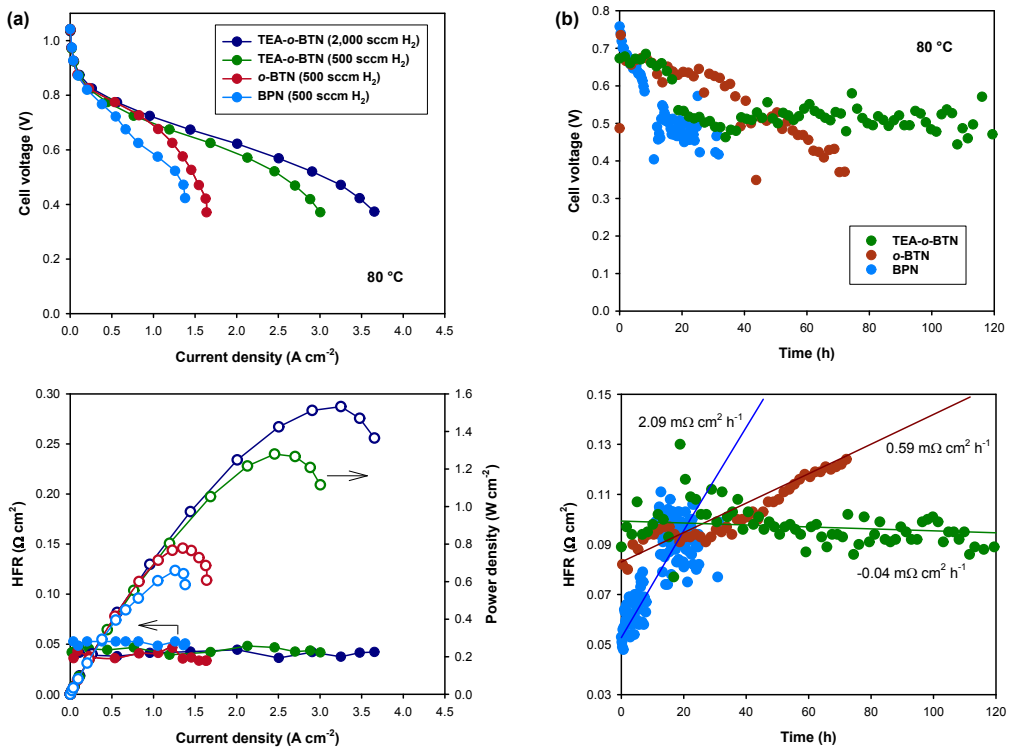

Fig. 5 (a) Impact of anode ionomer on AMFC performance. Measured the performance at 80 °C under H_2/O_2 (500/300 sccm, 2,000/1000 sccm) at 285 kPa backpressure. AEM: *m*-TPN (35 µm); anode: Pt-Ru/C (0.5 mg_{Pt} cm^{-2}); cathode: Pt/C (0.6 mg_{Pt} cm^{-2}), humidification: 100%. (b) Impact of anode ionomer on AMFC short-term stability of Pt anode catalysed MEAs. Measured the performance at 80 °C under H_2/O_2 (2000/300 sccm) at 147 kPa backpressure. AEM: *m*-TPN (24, 38, 35 µm thickness for the BPN, *o*-BTN, TEA-*o*-BTN cells, respectively); anode: Pt/C (0.6 mg_{Pt} cm^{-2}); cathode: Pt/C (0.6 mg_{Pt} cm^{-2}), humidification: 80%.

voltage and HFR changes during the short-term durability test. The fluctuation of the data was rather substantial because we applied the maximum H_2 flow rate of the mass flow controller. All MEAs exhibit a sharp drop in the initial stages of the durability test (~20 h). This is attributed to the oxidation of cathode ionomer at the high cell potential.[22] The BPN-based MEA failed to generate 0.6 A cm^{-2} current density after 32 h operation. The cell voltage of the MEA quickly reduced over time with accompanying rapid HFR increase (2.09 mΩ cm^2 h^{-1}). The *o*-BTN-based MEA exhibited higher stability; the cell was operated for 78 h before failure. The HFR increase rate for the *o*-BTN cell was lower (0.53 mΩ cm^2 h^{-1}). The TEA-*o*-BTN-based MEA did not reach to the operation failure point. The HFR of the TEA-*o*-BTN cell was stable (0.04 mΩ cm^2 h^{-1}). The results indicate cation-hydroxide-water co-adsorption was impeded by the introduction of steric hindrance of dimethyl group of o-BTN and further slowed down by the introduction of triethylammonium cation of TEA-*o*-BTN. Although the ultimate lifetime of the cells may be much longer with low voltage pulsing or cell replenishing process, these distinctive short-term voltage change behaviours of the cells provide an additional aspect of AMFC performance and durability. While the initial AMFC performance of the MEAs employing different anode ionomer is mostly affected by H_2 transport rate, the short-term durability of the MEAs is also affected by AEM dehydration as observed that the cell voltage loss was accompanied with HFR increase. Since the cell was operated at a constant current density (same amount of water generated) and under the fully humidified conditions, the gradual AEM dehydration over time should be related with the water transport at the anode which may be different depending on ionomer structure. As water transport is also proportional to the FFV of the polymer[51-53] and inversely proportional to the layer thickness of the co-adsorbed layer, we expect more stable AMFC cell performance with TEA-*o*-BTN-based MEA.

Conclusions

In our previous papers,[20, 24, 25] we have demonstrated that the adsorption of phenyl groups in the ionomeric binder on HOR catalysts may be the most detrimental factor for the performance of polyaromatic-based MEAs. As plausible solutions to minimize the undesirable phenyl adsorption have become available through less phenyl adsorbing polyaromatic ionomers and less phenyl adsorbed Pt-Ru bimetallic catalysts, we investigated the hydrogen transport issue, probably the second most significant performance limiting factor for the AMFC anode. For this study, we synthesized structurally modified BPN ionomers, targeting to improve hydrogen transport at the anode of AMFCs. Two strategic approaches have been made to improve hydrogen transport at the AMFC anode. The first approach is to increase the FFV of the quaternized BPN by introducing symmetric dimethyl groups in the polymer backbone. The prepared dimethyl substituted BPN, *o*-BTN, has significantly higher hydrogen diffusion coefficient measured from ^{1}H NMR and increases the peak power density of ~25% compared to that of the unsubstituted BPN. The second approach is to minimize cation-hydroxide-water co-adsorption on the HOR catalysts by replacing alkyl TMA functional group with alkyl TEA functional group. The microelectrode experiments exhibited the hydrogen limiting current of alkyl TEA functionalized dimethyl substituted BPN (TEA-*o*-BTN) was approximately two times higher than that of *o*-BTN. As a result of reduced cation group co-adsorption and increased hydrogen access to the HOR catalyst surface, the TEA-*o*-BTN based MEA have additional 60% improved peak power density at the same AMFC operating conditions. The performance improvement results suggest that the AMFC performance is more limited by slow hydrogen access due to the cation-hydroxide-water co-adsorption than by the low H_2 diffusion coefficient of BPN. Increasing the hydrogen flow rate to 2,000 sccm for TEA-*o*-BTN based MEA further increase the AMFC performance, reaching the peak power density to >1,500 mW/cm^2. However, our result showed that the hydrogen transport problem at the anode is not entirely resolved even with the TEA-*o*-BTN ionomer as we observed an increased cell performance with higher flow rate. This result emphasizes the importance of the selection of the cationic functional group in terms of H_2 permeability and provides insights into further design aspect of anode polymer electrolytes of AMFC.

Conflicts of interest

There are no conflicts to declare.

Acknowledgements

We thank Dr. Hoon Chung at LANL for helping the RDE experiments. This work was supported by the US Department of Energy, Energy Efficiency and Renewable Energy, Fuel Cell Technologies Office (FCTO). Los Alamos National Laboratory is operated by Triad National Security, LLC under U. S. Department of Energy Contract Number 89233218CNA000001.

Notes and references

1. S. Gottesfeld, D. R. Dekel, M. Page, C. Bae, Y. Yan, P. Zelenay and Y. S. Kim, *Journal of Power Sources*, 2018, **375**, 170-184.
2. J. R. Varcoe and R. C. T. Slade, *Electrochemistry Communications*, 2006, **8**, 839-843.
3. L. S. Liu, J. Ahlfield, A. Tricker, D. Chu and P. A. Kohl, *Journal of Materials Chemistry A*, 2016, **4**, 16233-16244.
4. H. Ono, J. Miyake, S. Shimada, M. Uchida and K. Miyatake, *Journal of Materials Chemistry A*, 2015, **3**, 21779-21788.
5. T. H. Pham, J. S. Olsson and P. Jannasch, *Journal of the American Chemical Society*, 2017, **139**, 2888-2891.
6. J. Y. Jeon, S. Park, J. Han, S. Maurya, A. D. Mohanty, D. Tian, N. Saikia, M. A. Hickner, C. Y. Ryu, M. E. Tuckerman, S. J. Paddison, Y. S. Kim and C. Bae, *Macromolecules*, 2019, **52**, 2139-2147.
7. C. Fujimoto, D. S. Kim, M. Hibbs, D. Wrobleski and Y. S. Kim, *Journal of Membrane Science*, 2012, **423**, 438-449.
8. J. T. Fan, A. G. Wright, B. Britton, T. Weissbach, T. J. G. Skalski, J. Ward, T. J. Peckham and S. Holdcroft, *Acs Macro Letters*, 2017, **6**, 1089-1093.
9. W. You, K. M. Hugar and G. W. Coates, *Macromolecules*, 2018, **51**, 3212-3218.

10. L. Zhu, J. Pan, C. M. Christensen, B. C. Lin and M. A. Hickner, *Macromolecules*, 2016, **49**, 3300-3309.
11. L. Liu, S. Q. He, S. F. Zhang, M. Zhang, M. D. Guiver and N. W. Li, *Acs Applied Materials & Interfaces*, 2016, **8**, 4651-4660.
12. Y. B. He, X. L. Ge, X. Liang, J. J. Zhang, M. A. Shehzad, Y. Zhu, Z. J. Yang, L. Wu and T. W. Xu, *Journal of Materials Chemistry A*, 2018, **6**, 5993-5998.
13. M. Mandal, G. Huang and P. A. Kohl, *ACS Applied Energy Materials*, 2019, **2**, 2447-2457.
14. H. G. Peng, Q. H. Li, M. X. Hu, L. Xiao, J. T. Lu and L. Zhuang, *J. Power Sources*, 2018, **390**, 165-167.
15. J. Wang, Y. Zhao, B. P. Setzler, S. Rojas-Carbonell, B. Yehuda, A. Amel, M. Page, L. Wang, K. Hu, L. Shi, S. Gottesfeld, B. Xu and Y. Yan, *Nature Energy*, 2019, **4**, 392-398.
16. S. D. Poynton, R. C. T. Slade, T. J. Omasta, W. E. Mustain, R. Escudero-Cid, P. Ocon and J. R. Varcoe, *Journal of Materials Chemistry A*, 2014, **2**, 5124-5130.
17. D. S. Kim, C. H. Fujimoto, M. R. Hibbs, A. Labouriau, Y. K. Choe and Y. S. Kim, *Macromolecules*, 2013, **46**, 7826-7833.
18. Y. Wang, G. W. Wang, G. W. Li, B. Huang, J. Pan, Q. Liu, J. J. Han, L. Xiao, J. T. Lu and L. Zhuang, *Energy & Environmental Science*, 2015, **8**, 177-181.
19. D. G. Li, I. Matanovic, A. S. Lee, E. J. Park, C. Fujimoto, H. T. Chung and Y. S. Kim, *Acs Applied Materials & Interfaces*, 2019, **11**, 9696-9701.
20. I. Matanovic, H. T. Chung and Y. S. Kim, *J. Phys. Chem. Lett.*, 2017, **8**, 4918-4924.
21. D. Li, H. T. Chung, S. Maurya, I. Matanovic and Y. S. Kim, *Curr Opin Electrochem*, 2018, **12**, 189-195
22. S. Maurya, A. S. Lee, D. Li, E. J. Park, D. P. Leonard, S. Noh, C. Bae and Y. S. Kim, *Journal of Power Sources*, 2019, **436**, 226866.
23. S. Maurya, S. Noh, I. Matanovic, E. J. Park, C. N. Villarrubia, U. Martinez, J. Han, C. Bae and Y. S. Kim, *Energy Environ. Sci.*, 2018, **11**, 3283-3291.
24. I. Matanovic, S. Maurya, E. J. Park, J. Y. Jeon, C. Bae and Y. S. Kim, *Chemistry of Materials*, 2019, **31**, 4195-4204.
25. S. Maurya, C. H. Fujimoto, M. R. Hibbs, C. N. Villarrubia and Y. S. Kim, *Chem. Mater.*, 2018, **30**, 2188-2192.
26. T. J. Omasta, L. Wang, X. Peng, C. A. Lewis, J. R. Varcoe and W. E. Mustain, *Journal of Power Sources*, 2018, **375**, 205-213.
27. H. T. Chung, U. Martinez, J. Chlistunoff, I. Matanovic and Y. S. Kim, *J. Phys. Chem. Lett.*, 2016, **7**, 4464-4469.
28. L. Q. Wang, E. Magliocca, E. L. Cunningham, W. E. Mustain, S. D. Poynton, R. Escudero-Cid, M. M. Nasef, J. Ponce-Gonzalez, R. Bance-Souahli, R. C. T. Slade, D. K. Whelligan and J. R. Varcoe, *Green Chemistry*, 2017, **19**, 831-843.
29. J. S. Mchattie, W. J. Koros and D. R. Paul, *Polymer*, 1991, **32**, 2618-2625.
30. J. S. Mchattie, W. J. Koros and D. R. Paul, *Polymer*, 1991, **32**, 840-850.
31. H. T. Chung, Y.-K. Choe, U. Martinez, J. H. Dumont, A. Mohanty, C. Bae, I. Matanovic and Y. S. Kim, *J. Electrochem. Soc.*, 2016, **163**, F1503-F1509.
32. M. Dunwell, J. H. Wang, Y. Yan and B. Xu, *Physical Chemistry Chemical Physics*, 2017, **19**, 971-975.
33. W.-H. Lee, Y. S. Kim and C. Bae, *ACS Macro Letters*, 2015, **4**, 814-818.
34. E. J. Park and Y. S. Kim, *J. Mater. Chem. A*, 2018, **6**, 15456-15477.
35. J. Y. Park and D. R. Paul, *Journal of Membrane Science*, 1997, **125**, 23-39.
36. J. H. Dumont, R. P. Hjelm, E. B. Watkins, H. T. Chung, U. P. Martinez, P. Atanassov and Y. S. Kim, presented in part at the 230th ECS Meeting, October 4, 2016.
37. A. R. Cruz, M. C. G. Hernandez, M. T. Guzman-Gutierrez, M. G. Zolotukhin, S. Fomine, S. L. Morales, H. Krichedorf, E. S. Wilks, J. Cardenas and M. Salmon, *Macromolecules*, 2012, **45**, 6774-6780.
38. H. Gao, J. Li and K. Lian, *RSC Advances*, 2014, **4**, 21332-21339.
39. D. R. Dekel, M. Amar, S. Willdorf, M. Kosa, S. Dhara and C. E. Diesendruck, *Chemistry of Materials*, 2017, **29**, 4425-4431.
40. E. J. Park, S. Maurya, M. R. Hibbs, C. H. Fujimoto, K.-D. Kreuer and Y. S. Kim, *Macromolecules*, 2019, DOI: 10.1021/acs.macromol.9b00853.
41. M. G. Marino and K. D. Kreuer, *ChemSusChem*, 2015, **8**, 513-523.
42. G. R. Fulmer, A. J. M. Miller, N. H. Sherden, H. E. Gottlieb, A. Nudelman, B. M. Stoltz, J. E. Bercaw and K. I. Goldberg, *Organometallics*, 2010, **29**, 2176-2179.
43. E. Sartori, M. Ruzzi, N. J. Turro, J. D. Decatur, D. C. Doetschman, R. G. Lawler, A. L. Buchachenko, Y. Murata and K. Komatsu, *Journal of the American Chemical Society*, 2006, **128**, 14752-14753.
44. J. Harmon, C. Coffman, S. Villarrial, S. Chabolla, K. A. Heisel and V. V. Krishnan, *Journal of Chemical Education*, 2012, **89**, 780-783.
45. P. Stilbs, *Progress in Nuclear Magnetic Resonance Spectroscopy*, 1987, **19**, 1-45.
46. W. S. Price, *Concepts in Magnetic Resonance*, 1997, **9**, 299-336.
47. M. D. Pelta, G. A. Morris, M. J. Stchedroff and S. J. Hammond, *Magnetic Resonance in Chemistry*, 2002, **40**, S147-S152.
48. W.-H. Lee, E. J. Park, J. Han, D. W. Shin, Y. S. Kim and C. Bae, *ACS Macro Letters*, 2017, **6**, 566-570.
49. S. D. Yim, H. T. Chung, J. Chlistunoff, D. S. Kim, C. Fujimoto, T. H. Yang and Y. S. Kim, *Journal of the Electrochemical Society*, 2015, **162**, F499-F506.
50. P. Ruetschi, *Journal of the Electrochemical Society*, 1966, **113**, C200-&.
51. T. C. Merkel, B. D. Freeman, R. J. Spontak, Z. He, I. Pinnau, P. Meakin and A. J. Hill, *Chemistry of Materials*, 2003, **15**, 109-123.
52. S. J. Lue, D. T. Lee, J. Y. Chen, C. H. Chiu, C. C. Hu, Y. C. Jean and J. Y. Lai, *J Membrane Sci*, 2008, **325**, 831-839.
53. G. M. Shi, H. M. Chen, Y. C. Jean and T. S. Chung, *Polymer*, 2013, **54**, 774-783.